JACS
JOURNAL OF THE AMERICAN CHEMICAL SOCIETY
Article
Cite This: J. Am. Chem. Soc. 2017, 139, 16630-16639
pubs.acs.org/JACS

# Template-Free Hierarchical Self-Assembly of Iron Diselenide Nanoparticles into Mesoscale Hedgehogs

Dawei Deng,[†,‡] Changlong Hao,[▽] Soumyo Sen,[#] Chuanlai Xu,[▽] Petr Král,[#] and Nicholas A. Kotov*[,†,∥,§,⊥]

[†]Department of Chemical Engineering, [∥]Department of Biomedical Engineering, [§]Department of Materials Science and Engineering, and [⊥]Biointerface Institute, University of Michigan, Ann Arbor, Michigan 48109, United States

[‡]School of Life Science and Technology, and State Key Laboratory of Natural Medicines, China Pharmaceutical University, Nanjing 210009, P. R. China

[▽]School of Food Science and Technology, State Key Lab of Food Science and Technology, Jiangnan University, Wuxi, Jiangsu 214122, P. R. China

[#]Department of Chemistry, Physics and Biopharmaceutical Sciences,, University of Illinois at Chicago, Chicago, Illinois 60607, United States

Supporting Information

**ABSTRACT:** The ability of semiconductor nanoparticles (NPs) to self-assemble has been known for several decades. However, the limits of the geometrical and functional complexity for the self-assembled nanostructures made from simple often polydispersed NPs are still continuing to amaze researchers. We report here the self-assembly of primary ~2−4 nm $FeSe_2$ NPs with puck-like shapes into either (a) monocrystalline nanosheets ~5.5 nm thick and ~1000 nm in lateral dimensions or (b) mesoscale hedgehogs ~550 nm in diameter with spikes of ~250 nm in length, and ~10−15 nm in diameter, the path of the assembly is determined by the concentration of dodecanethiol (DT) in the reaction media. The nanosheets represent the constitutive part of hedgehogs. They are rolled into scrolls and assembled around a single core with distinct radial orientation forming nanoscale "needles" approximately doubling its fractal dimension of these objects. The core is assembled from primary NPs and nanoribbons. The size distribution of the mesoscale hedgehogs can be as low as 3.8%, indicating a self-limited mechanism of the assembly. Molecular dynamics simulation indicates that the primary $FeSe_2$ particles have mobile edge atoms and asymmetric basal surfaces. The top-bottom asymmetry of the puck-like NPs originates from the Fe-rich/Se-rich stripes on the (011) surface of the orthorhombic $FeSe_2$ crystal lattice, displaying 2.7 nm periodicity that is comparable to the lateral size of the primary NPs. As the concentration of DT increases, the NPs bind to additional metal sites, which increases the chemical and topographic asymmetry and switches the assembly pathways from nanosheets to hedgehogs. These results demonstrate that the self-assembly of NPs with non-biological surface ligands and without any biological templates results in morphogenesis of inorganic superstructures with complexity comparable to that of biological assemblies, for instance mimivirus. The semiconductor nature of $FeSe_2$ hedgehogs enables their utilizations in catalysis, drug delivery, optics, and energy storage.

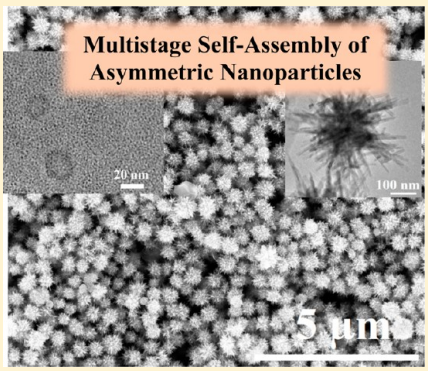


## INTRODUCTION

Despite decades of research on the self-assembly of nanoparticles (NPs), the spontaneous morphogenesis of inorganic nanoscale materials remains a scientific frontier relevant to both fundamental problems such as origin of life and current technological pains such as safe energy storage devices. From the template-directed organization of NPs,[1−5] the studies transitioned to template-free conditions when nanoscale assemblies emerge in the bulk of the solvent. For such nanocolloidal systems with unrestricted Brownian motion, the common self-organization patterns are known to be chains, sheets, ribbons, and helices,[6−8] as well as a diverse spectrum of gels,[9,10] supraparticles,[11−14] and superlattices.[15−19] The forces determining the spontaneous morphogenesis of NP superstructures are only partially understood,[6,20−24] whereas the limits of their complexity are unknown. Concomitantly, the demand for sophistication of the nanoscale assemblies is increasing due to the expectations of equally sophisticated chemical, optical, electrical, mechanical, and biological functionalities. To name a few examples when geometrical complexity of nanoscale structures of inorganic materials begets new functions, the specific and often counterintuitive three-dimensional (3D) positioning of plasmonic and excitonic particles results in multipole effects.[25−28] Corrugated interfaces with nanoscale roughness produce unexpected wetting[29−31]

Received: July 26, 2017
Published: October 10, 2017



DOI: 10.1021/jacs.7b07838
J. Am. Chem. Soc. 2017, 139, 16630−16639

and solvation[32] phenomena, while intricate molecular, nanoscale, and mesoscale shapes enable selective gas absorption, biomimetic catalysts, drug delivery vehicles, and stimuli-responsive gels.

Complex self-assembly patterns are well-known from biology[33−35] and many of them mirror those seen for inorganic NPs. Their formation is the product of assembly of often identical biological units with nanoscale dimensions organized into hierarchical constructs spanning several orders of dimensions.[36−40] The following question then inevitably emerges: *Are similar levels of complexity and hierarchy possible for non-biological building blocks?* A large library of NPs with different shapes[25,41−43] and a large spectrum of self-organized structures with gradually increasing degrees of complexity indicate feasibility of inorganic nanoscale structures with sophistication of geometry and function approaching those to their biological counterparts[35] when NPs possess a certain degree of anisotropy and dynamic structural reconfiguration.[6,44−49] The answer(s) to this question have broad technological impacts because harnessing self-organization will l (a) improve energy efficiency of device manufacturing, (b) bridge nanoscale materials with microscale technologies, and (c) simplify the realization of complex mesoscale "machines".[50−52]

Here we found that 2−5 nm puck-shaped NPs of iron diselenide $FeSe_2$ are capable of self-assembly into 550 nm particles with hedgehog-like morphology and uniform size distribution. The previous preparative method for hedgehog particles included growing ZnO nanowires on a microscale polystyrene core.[32] Self-organization route for hedgehogs would certainly be desirable due to its simplicity although at the start of the project seemed highly unlikely because they incorporate at least three assembly patterns that must be coordinated in a specific fashion: assembly of the core, assembly of the needles, and assembly of the needles around the core. Nevertheless, one-pot assembly of hedgehogs is possible; the chemical conditions enabling such multistage self-assembly were found by judicious selection of the ratio and concentration for the two surface ligands: oleylamine (OLA) and dodecanethiol (DT) in 1-octadecene (ODE). For $FeSe_2$ NPs sparsely covered with DT surface ligands nanosheets are formed. For the same NPs more densely coated with DT, the top/bottom asymmetry of the primary puck-like particles is increased and hedgehogs start forming. "Needles" of these hedgehogs are constructed as rolled monocrystalline $FeSe_2$ nanosheets extending from the central core. The latter are self-limited spheroids self-organized from the primary NPs and nanoribbons. The experimental and computational data about the early stages of the assembly point to multistage hierarchical assembly leading to the complex geometry of mesoscale hedgehogs.

While our interest in this study is primarily fundamental, the mesoscale $FeSe_2$ hedgehog particles are also technologically significant. The specific advantage of their unusual geometry is related to anomalous dispersion behavior of particles with highly corrugated surfaces.[32] The continuous crystallinity resulting from oriented attachment[6,45,53−55] and the semiconductor properties of $FeSe_2$ (1.0 eV band gap and absorption coefficient of $5 \times 10^5$ $cm^{-1}$)[56−59] also make them promising high performance light absorbers,[60] battery anodes,[61] nonlinear optical materials,[62] and catalysts.[63,64] The hierarchical biomimetic self-assembly process simplifies their scalable manufacturing.

## RESULTS AND DISCUSSION

**Synthesis of Constitutive NPs.** Self-assembly of NPs from iron chalcogenides received relatively little attention compared with similar processes involving gold-, cadmium-, or lead-based NPs although $FeS_2$ and $FeSe_2$ represent some of the most promising energy storage and catalytic nanomaterials today.[54,65−71] The choice of the NP material for this study was also based on the early observations of corrugated iron chalcogenide nanostructures.[72−76] Their geometrical complexity might be further increased by deliberate engineering of the synthetic pathway via self-assembly of nanoscale particles. In comparison with self-assembly of NPs from PbS[77] and Au[78] with cubic or hexagonal crystal lattice, the same processes involving iron chalcogenides could lead to more complex superstructures because orthorhombic crystal lattice of the latter is more asymmetric, which must increase the anisotropy of the primary NPs.

Considering previous studies of $FeSe_2$[60−64] and $FeS_2$[54,65−71,79] nanostructures, we chose organic media for synthesis in this instance, namely in the mixture of DT and OLA in ODE,[79−81] due to greater stability of $FeSe_2$ against oxidation in these solvents than in water and previous expertise.[62] Besides coordinating the NP surface, these surface ligands also have reductive properties. Starting with $Fe^{3+}$, namely anhydrous $FeCl_3$, chalcogenides of $Fe^{2+}$ can be obtained.

When the concentration of DT in ODE during the synthesis is low, namely [DT] = 67.5 mmol/L, $FeSe_2$ nanosheets are formed (Figure 1a). As the concentration of DT increased six times to [DT] = 405 mmol/L compared to the previous conditions, one can observe the transition from the formation of nanosheets to corrugated mesoscale spheres (Figure 1b). When the amount of DT is increased 10 times, namely [DT] = 675 mmol/L, mesoscale hedgehog particles with a diameter of 550 ± 20 nm are exclusively produced (Figure 1c). Hedgehog particles retain their dominance as DT concentration becomes even higher albeit increasing the diameter of the needles.

Reaction optimization was carried out further for two additional parameters: the temperature of the reaction and OLA concentration (Figures S1−S5) to maximize the yield of either nanosheets or hedgehogs. The optimal volumes of DT and OLA in solution A (see Methods) for formation of nanosheets are 0.1 and 2 mL, respectively. The optimal volumes of DT and OLA for formation of mesoscale hedgehogs are 1 and 2 mL, respectively. The optimal temperature for both products was found to be 175 °C. The parameter matrix and corresponding composition of the products indicate that the primary parameter controlling the switch between formation of nanosheets and hedgehogs is the DT concentration.

Mesoscale $FeSe_2$ hedgehog particles display some morphological analogy with a variety of star-like particles,[25,28,77,81,82] with exception that the aspect ratio of the "rays" (also called needles) is greater. The outer diameters of the hedgehogs reveal notable size-uniformity with dispersity index as low as 3.8% as established by the image processing with the shape recognition of the electron microscopy data followed by the statistical analysis (Figure 1f). High size uniformity of the hedgehogs is indicative of the self-limitation mechanism of their formation.[11,83] Mesoscale hedgehogs exhibit absorption and scattering in a wide spectral region ranging from visible (vis) to near-infrared (NIR) (Figure S2a) that is similar to extinction spectra of microscale hedgehogs.[32]



DOI: 10.1021/jacs.7b07838
J. Am. Chem. Soc. 2017, 139, 16630−16639

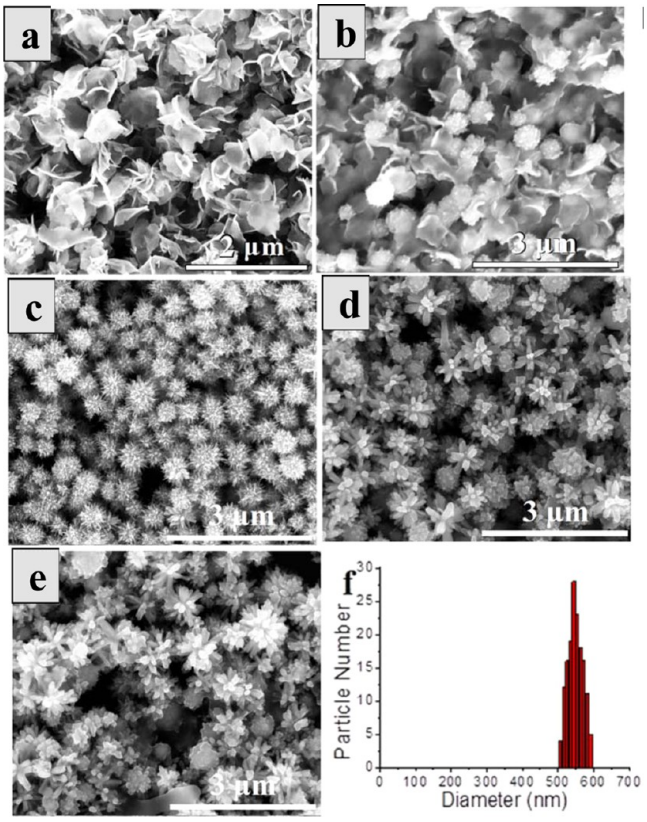


**Figure 1.** SEM images of the $FeSe_2$ nanostructures for different amounts of DT in "solution A": (a) 0.1, (b) 0.6, (c) 1.0, (d) 2.0, and (e) 4.0 mL. The amount of OLA was fixed at 2 mL; the volume of ODE was adjusted to keep the total volume of "solution A" constant at ~6 mL. (f) Size distribution of the $FeSe_2$ hedgehogs. The average size of hedgehogs is 550 ± 20 nm.

**Self-Assembly of Primary $FeSe_2$ NP into Nanosheets.** Formation of nanosheets of $FeSe_2$ are scientifically interesting because of the current widely spread research on 2D semiconductor nanomaterials. However, in the framework of this study, we shall focus primarily on $FeSe_2$ hedgehogs. The mechanism of the nanosheet formation is, important from this standpoint as well because it is permits deciphering the mechanism of hedgehog formation.

The metal-to-chalcogen atomic ratio in perfect $FeSe_2$ lattice is 1:2. OLA and DT ligands bind to metal sites; thus, they coat the NP surface more sparsely than a typical semiconductor NPs with metal-to-chalcogen ratio of 1:1, for instance PbS, CdSe, or CdTe.[79] Furthermore, DT and OLA surface ligands on NPs are expected to be labile and, given sufficient thermal activation, they are likely to go on and off the NP surface. According to EDX spectrum, nanosheets have atomic ratio of Fe:Se:S = 1:2.1:0.05 (Figure S6b). The deviation from the $FeSe_2$ stoichiometry is representative of the contribution of surface ligands to the chalcogenide lattice of these nanostructures. The attribution of $FeSe_2$ as the chemical formula to these nanostructures is, therefore, an approximation. The fact that considerable doping taking place can be further supported by the weakness or lack of fluorescence at room temperature associated with efficient quenching of excited states due to adatoms (Figure S10).

The formation of monocrystalline $FeSe_2$ nanosheets with flat and curled geometry (Figures 2, 3, and S8) were observed. In both cases, their lateral size and thickness were ~600−1000 nm

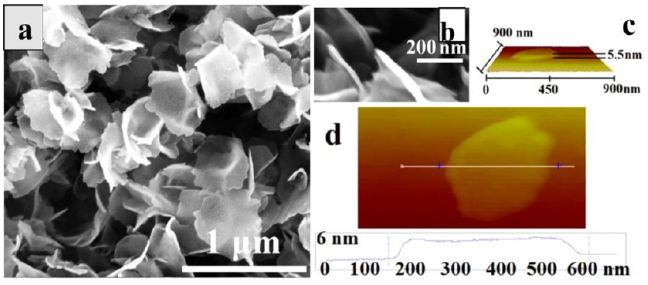


**Figure 2.** (a) Top and (b) side view SEM images of $FeSe_2$ nanosheets. (c) AFM image and (d) corresponding topography cross section (~5.5 nm in thickness) of a nanosheet. Additional images are shown in Figure S7.

and ~5.5 nm, respectively (Figures 2, S6, and S7). Nanosheets were monocrystalline (Figures 3 and S9) with atomic packing corresponding to orthorhombic phase of $FeSe_2$ (JCPDS No. 21-0432). Based on the observed electron diffraction patterns, the vector of the incident electron beam was aligned with [11−1] axis in $FeSe_2$ lattice. Hence, the three preferential growth directions are (011), (101) and (1−10) planes of $FeSe_2$ orthorhombic lattice (Figure 3b).

To learn more about the growth mechanism, we monitored the intermediate stages of nanosheet formation (Figures S11−S14). The growth pattern presented in Figure 4 is similar to that of previous $FeSe_2$ nanosheets formed in DMSO.[69] At the earliest time point after the injection of Se precursor (30 s), the puck-shaped NPs formed that will be referred to as "primary" NPs because they precede the formation of all the other structures in this nanocolloidal system. These NPs are small and active rapidly assembling into planar aggregates ~30−100 nm in size (Figure 4a). The approximate lateral size the primary NPs is ~2−3 nm based on the individual crystallites seen soon after injection of the Se precursor and the dimensions of crystalline domains in the early nanosheets (Figure 4). The planar agglomerates grow along the lateral dimensions reaching ~150−300 nm in diameter (Figure 4b) retaining the same thickness. Based on AFM images, the thickness of the nanosheets is ~5.5 nm throughout the assembly process indicating preferential edge-to-edge attachment of the primary NPs.[84] Since AFM height measurements also include the surface ligands, this thickness is consistent with the dimensions of single primary NPs and particle-by-particle assembly,[45,54,69] rather than the atom-by-atom growth process.[85]

Cumulatively, the schematic of the assembly of primary NPs into nanosheets is given in Figure 5. The basal surfaces of the nanosheets and the primary NPs have a normal parallel to the [11−1] axis of orthorhombic $FeSe_2$ lattice (Figure 5b), which was consistent with the data in Figure 3. The coalescence of primary NPs occurs via the fusion of the (011), (101), and/or (1−10) facets. One cannot expect that the primary NPs have perfect geometrical match to each other or very uniform in lateral size. Considering the monocrystallinity of the resulting sheets, there must be some atomic-scale reorganization at the edges of the NPs as they self-assemble, which must be involved in self-assembly process in addition to oriented attachment.[45,53,54,69]

**Self-Assembly of Primary $FeSe_2$ NPs into Mesoscale Hedgehog Particles.** DT surface ligands adsorb selectively on specific faces of NPs[86,87] leading to anisotropy of van der Waals, hydrophobic, and electrostatic (charge−charge, dipole−dipole, and ion−dipole) interactions. Even minor anisotropy of


DOI: 10.1021/jacs.7b07838
J. Am. Chem. Soc. 2017, 139, 16630−16639

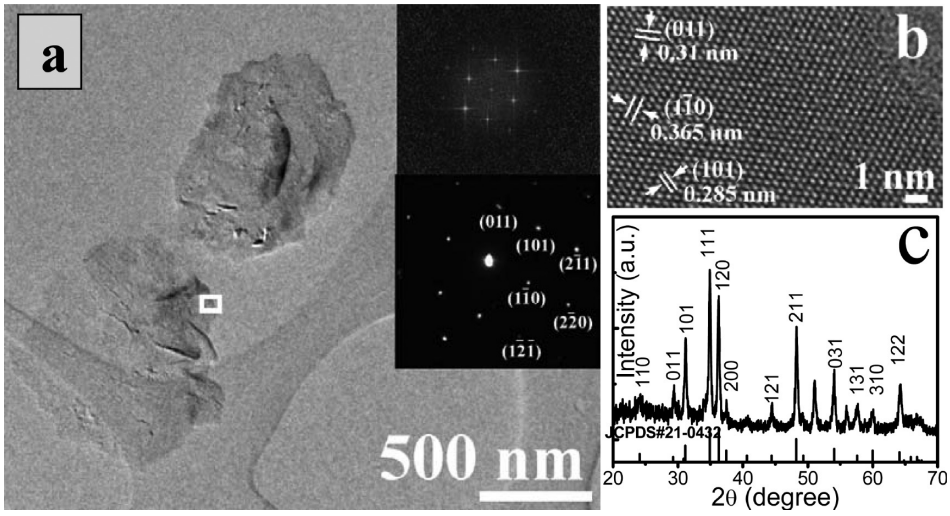


**Figure 3.** (a) TEM and (b) HR-TEM images of $FeSe_2$ nanosheets. Insets of panel (a) are the corresponding fast Fourier transform (FFT) and selected area electron diffraction (SAED) patterns. (c) Powder XRD pattern of nanosheets. The three *d*-spacings in panel (b) are 3.65, 3.1, and 2.85 Å, corresponding to the (110), (011), and (101) lattice planes of orthorhombic $FeSe_2$, respectively.

these interactions is known to lead to complex nanoscale structures from NPs.[24,88] The $FeSe_2$ hedgehog particles display unusually high monodispersity and geometrical complexity with their branches/rays emanating from a common origin (Figures 6 and S15). The distinct hedgehog geometry of the spontaneously formed particles was confirmed by the TEM tomography (Figures 6c and S18, and Video File S1). Unlike nanoscale star-like and microscale hedgehog particles made previously,[25,28,32,77,81,82] the "rays" or "needles" in these assemblies are hollow (Figure 6f) being the scrolled version of the nanosheets from Figure 2. As one measure of their complexity, the fractal dimension, $D_f$, of the two contours for the projections of the TEM images for the hedgehog particles is ~1.75 as compared to $D_f \approx 1$ for the nanosheets. For the larger hedgehogs, the morphology of scrolled $FeSe_2$ sheets could be observed even by SEM (Figure S16). The dimensions of the nanoscrolls are ~250 nm in length, ~10−15 nm in diameter, and ~2 nm in wall thickness.

The EDX spectrum revealed the elemental composition of $FeSe_2$ to be Fe:Se:S = 1:2.2:0.2 (Figure S15b), which is similar to that of nanosheets with exception of increased atomic percentage of sulfur which is associated with greater density of DT surface ligand on the surface of mesoscale hedgehogs than on nanosheets. Weak broad-band photoluminescence of mesoscale hedgehogs was observed in the 400−500 nm spectral window (Figures S14 and S17).

High-resolution TEM (Figure 7) confirmed single-crystal structure of the $FeSe_2$ nanoscrolls forming the "needles". Three sets of lattice fringes were observed, corresponding to the (1−10), (011), and (101) lattice planes of orthorhombic $FeSe_2$, which suggests that the nanoscrolls are rolled up along the axis that is perpendicular to [11−1] and parallel to (1−10). The powder XRD pattern also verifies the orthorhombic phase of $FeSe_2$ (Figure 7c).

**Mechanistic Insights.** The formation of $FeSe_2$ hedgehogs cannot be explained by the ion-by-ion growth models of the NPs. It must be driven by the interparticle forces. Once this conclusion is made, it is clear that it is difficult to offer at the moment a theoretical or simulation framework that can give full or even intermediate level of mechanistic details for the formation of such complex structures from molecular precursors. The bottleneck in describing the mechanism is associated with the steps involving transition of the primary NPs into the mesoscale superstructures. The problems originate from the complexity of the close-range NP interactions that cannot be quantitatively described by the existing theories.[24] Atomistic molecular dynamics (MD) simulations can, in principle, account for non-additivity and dynamics of NP interactions, but have difficulties in accommodating sufficiently long times and sufficiently large number (thousands) of NPs characteristic of the actual assembly processes.[89] Coarse-grained simulations offer the powerful toolbox for modeling NPs systems with adequately scaled times and sufficiently large number of NPs, but parametrization of NP interactions in them requires diligent adaptation to specific nanoscale system guided by empirical observations.[7,11,90,91] Both simulation techniques can yield excellent matches with geometries of a subset of the experimental assemblies although not yet as complex as hedgehogs.[11,83,92,93] The hybrid methods combining quantum mechanical, density functional theory, MD, and coarse-grained or Monte Carlo algorithms are promising in their accuracy[89,94] but so far have not been implemented for multistage hierarchical assemblies.

Within the confines of this paper, we shall make the first steps toward elucidating the mechanism of NPs → hedgehogs transition looking for a conceptual framework to answer the following question: *How can such geometrically complex system with characteristic dimensions exceeding 500 nm self-assemble from pieces 2−3 nm in size?* From this standpoint, we decided to identify the intermediate stages of the assembly. To accomplish it the reactions was carried out in some instances at 150 °C (Figure S20) instead of 175 °C to gain the information about the very early stages of NP assembly better. Based on the microscopy data in Figures 2−4, 8, S19, and S20, the assembly process of the $FeSe_2$ hedgehog particles includes at least four stages: (i) formation of primary ~2−4 nm $FeSe_2$ NPs from $FeCl_3$, DT, and OLA (Figures 4a(i), 5a, S20a,b, and S21b); (ii) fusion of the primary NPs into short nanoribbons and spiky agglomerates (Figures 8a, S20c,d, and S23); (iii) assembly of the short ribbons and primary NPs around the spiky agglomerates into supraparticles[23] forming the cores of the


DOI: 10.1021/jacs.7b07838
J. Am. Chem. Soc. 2017, 139, 16630−16639

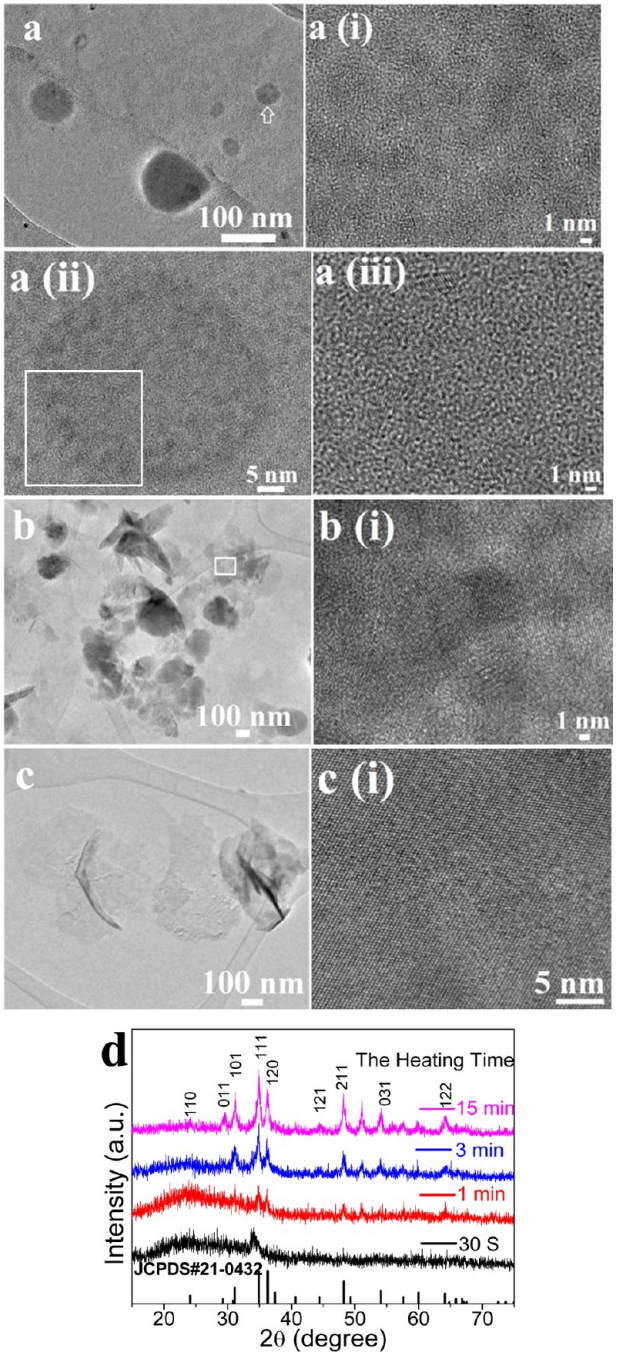


**Figure 4.** TEM images of reaction aliquots at 175 °C: (a) 30 s, (b) 1 min, and (c) 3 min. (d) XRD patterns of the intermediate stages of the nanosheet assembly. TEM images with consecutively higher magnification of early stages of nanosheet assemblies: (a(i)) HR-TEM image of primary NPs, (a(ii) and a(iii)) HR-TEM images of an early planar aggregate [white arrow in panel (a) marks the location of panel (a(ii)); white rectangle in panel (a(ii)) marks the location of panel (a(iii))]. (b(i)) HR-TEM image of the intermediate nanosheet with visible crystallites corresponding to primary NPs. (c(i)) HR-TEM image of the resulting $FeSe_2$ nanosheet.

hedgehogs (Figure 8c,d); and (iv) growth of the scrolls on the surface away from the surface of the supraparticle producing final hedgehogs (Figures 8e–h, S20e,f, and S23e,f). These stages overlap in time, and, for instance, the growth of hedgehog spikes and the completion of the core are likely to proceed simultaneously depending on the overall reagent concentrations (Figure S5) and local conditions.

Some parts of the mechanism of hedgehog assembly are familiar although for each such part one can find parts that are hard-to-explain. Among the former ones, is the monocrystallinity of nanosheets, nanoribbons, and nanoscrolls. Both TEM and XRD patterns confirms the presence of large monocrystalline domains in the mesoscale hedgehogs (Figure 8i). The single crystal nature of the key structural elements of the hedgehogs is a consequence of the edge-to-edge fusion of the primary NPs. The transition of NPs to nanoribbons also mirrors the past observation of the NPs → nanoribbons processes for CdTe,[7] PbS,[45] $FeS_2$,[69] $Cu_2S$,[98] and CdSe.[85]

The hard-to-explain aspect of this process is the distinct tendency to scroll. While rolled structures were also observed for some nanomaterials,[93,95−,99101] the nanosheets were not observed to spontaneously roll up in dispersion, in the absence of external stimuli, such as surface forces, mechanical strains, or thermal gradients.[96−98,102,103] Furthermore, the data in Figures 6−8 and S20e,f, are consistent with direct transition of nanoribbons into scrolls rather than the initial formation of the large sheets that subsequently roll up. No formation of adequately large sheets and partial scrolls are observed for conditions of hedgehogs formation (Figures 6−8, S20, S21, and S23).

The second part that is relatively well understood is the assembly of the NPs into self-limited aggregates with high uniformity.[11−14,77,92,104−108] Among potentially several structural elements, self-limited assemblies are represented here by the $FeSe_2$ cores. The hard-to-explain part here is the change from the space filling assembly pattern typical for standard supraparticles to the regularly spaced needles, that cannot be easily explained based on the models used before.[11,12,14,77,92,104−107] So, despite some familiar mechanisms of self-organization, the following sections needs to be treated as our best guesses about the mechanism of hedgehog morphogenesis.

Let us recall that the hedgehogs form when the concentration of DT is increased to about 10-fold, compared to that for nanosheets. Thus, the ligand density on the NPs surface is markedly (10×) increased which was affirmed by EDX spectra and the amplitudes of the sulfur peaks in Figures S6b and S15b. Higher ligand density on NPs and its significance for NP-NP interactions can also be visualized by the formation of a gel, whereas for NPs made at lower concentration of DT, no gelation is observed (Figure S22).

The increase of DT density on NP surfaces may increase the asymmetry between the two top/bottom sides of the puck-like $FeSe_2$ NPs. The main reason for the asymmetry is the peculiar structure of [1−11] surface of orthorhombic $FeSe_2$. The basal [1−11] planes for the primary NPs have alternating Se-rich and Fe-rich stripes (Figures 9). For long $FeSe_2$ nanoribbons and nanosheets, the total number of each type of Se-rich and Fe-rich stripes on both basal planes will be the same. However, the primary $FeSe_2$ NPs (~2 nm, Figures 8b and S21) are smaller than the period ~2.7 nm of the stripes (Figure 9 a,b) and thus their basal planes will not be identical. Even relatively large early NPs of ca. 7−8 nm in diameter that can accommodate more stripes will retain a part of this anisotropy because the numbers of Fe-rich stripes remains unequal between the top and the bottom surface (Figures 9a,b and 10b,c).

Asymmetry of primary NPs caused by the DT stripes can be illustrated by atomistic MD simulations (Video Files S2 and 3)


DOI: 10.1021/jacs.7b07838
J. Am. Chem. Soc. 2017, 139, 16630−16639

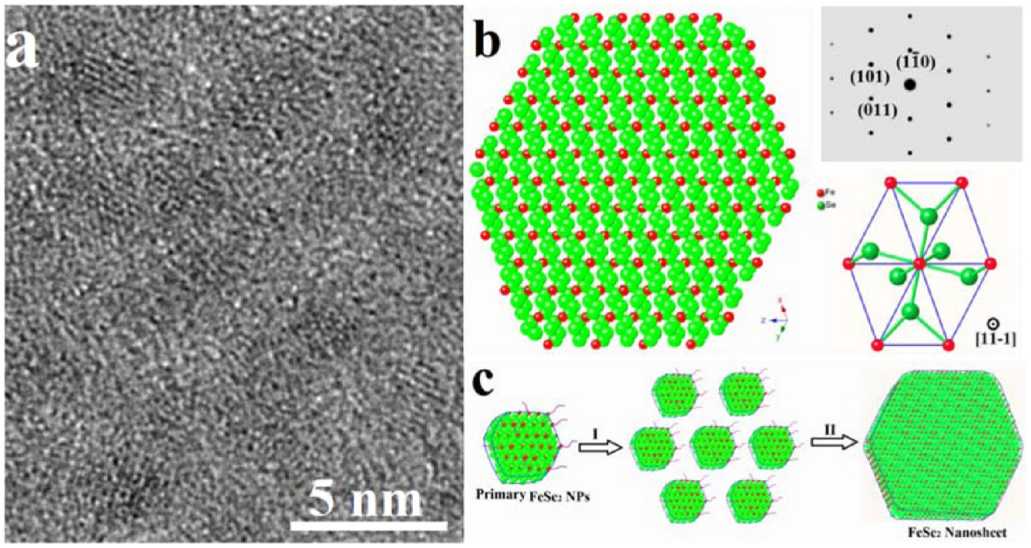


**Figure 5.** (a) HR-TEM image of primary puck-like NPs. (b) Atomic model (top view) of the orthorhombic $FeSe_2$ nanosheet viewed from its [11−1] axis. Upper-right inset: single-crystal diffraction pattern. Lower-right inset: unit cell structure of an orthorhombic ($FeSe_2$) lattice viewed from the [11−1] axis. (c) Schematic illustration of the assembly of the primary NPs into the nanosheets.

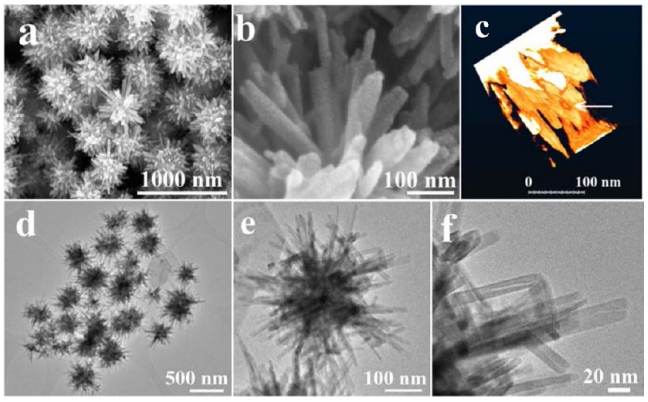


**Figure 6.** (a,b) SEM and (d,e) TEM images with increased magnification. (c) TEM tomography image of the assembled nanoscroll marked by an arrow in a mesoscale hedgehog particle (scale bar, 100 nm).

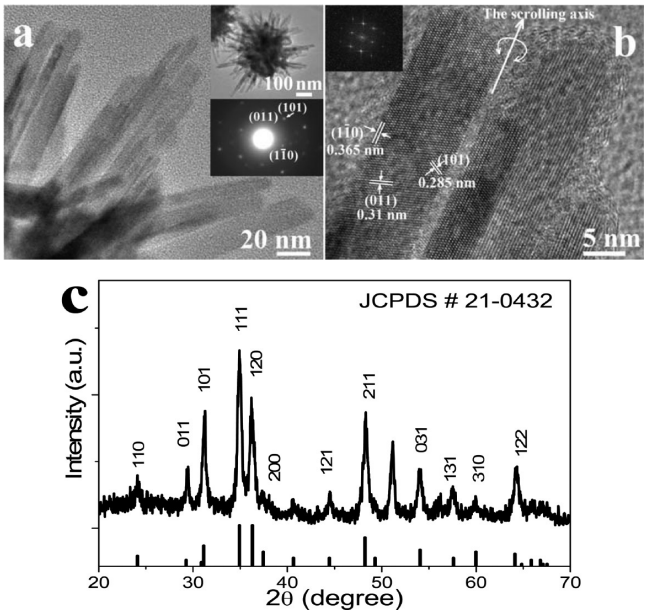


**Figure 7.** (a) TEM and (b) HR-TEM (inset: corresponding FFT pattern) images of $FeSe_2$ nanoscrolls in one assembled hedgehog particle (upper inset of panel (a)). The SAED pattern (lower inset of panel (a)) is consistent with the FFT pattern. (c) The corresponding powder XRD pattern.

of $FeSe_2$ plates of several nm representing the early NPs in Figures 5a, 8b, and 9d. The top-bottom anisotropy of the primary NPs, can also be described in term of patches produced by the DT "tails" (Figure S23). As was demonstrated *in silico*, pattern of patches may result in complex structures.[109] As one of the potential consequences, the patchiness may lead, for instance, to curling because the preferential concentration of the tails on one side would necessarily cause the bending as NPs are attaching to each (Figure S24). The preference for the non-planar configuration during the assembly process can be seen in the atomistic MD simulations for the two primary NPs in close vicinity of each other (Video File S4).

Analogous assembly patterns of the primary NPs into the curved nanoscale structures were observed for Au NPs.[93] The possibility of the formation of scrolls by the edge-to-edge assembly of primary NPs was also observed for $ReSe_2$.[110] Minimization of the surface tension was suggested as the driving force for curling. Whether the curved assembly pattern originates from unequal distribution of the DT patches or surface tension effects, it can be generalized as maximization of the van-der-Waals attraction of the sheets counteracted by the mechanical deformation of the semiconductor sheet and the surface layer. Considering that multiplicity of scrolled nanoscale structures were observed in the past,[95−103] such assembly pattern and force balances can be common for different self-organizing nanoscale systems.

## CONCLUSIONS

The multistage assemblies of $FeSe_2$ NPs into nanosheets and mesoscale hedgehog particles was observed. The spikes of hedgehogs are formed from the scrolled nanosheets that attach to the supraparticle core via one of the ends. The uniformity of mesoscale hedgehogs originates from the self-limitation of their growth. The anisotropy of the primary 2−3 nm NPs is


DOI: 10.1021/jacs.7b07838
J. Am. Chem. Soc. 2017, 139, 16630−16639

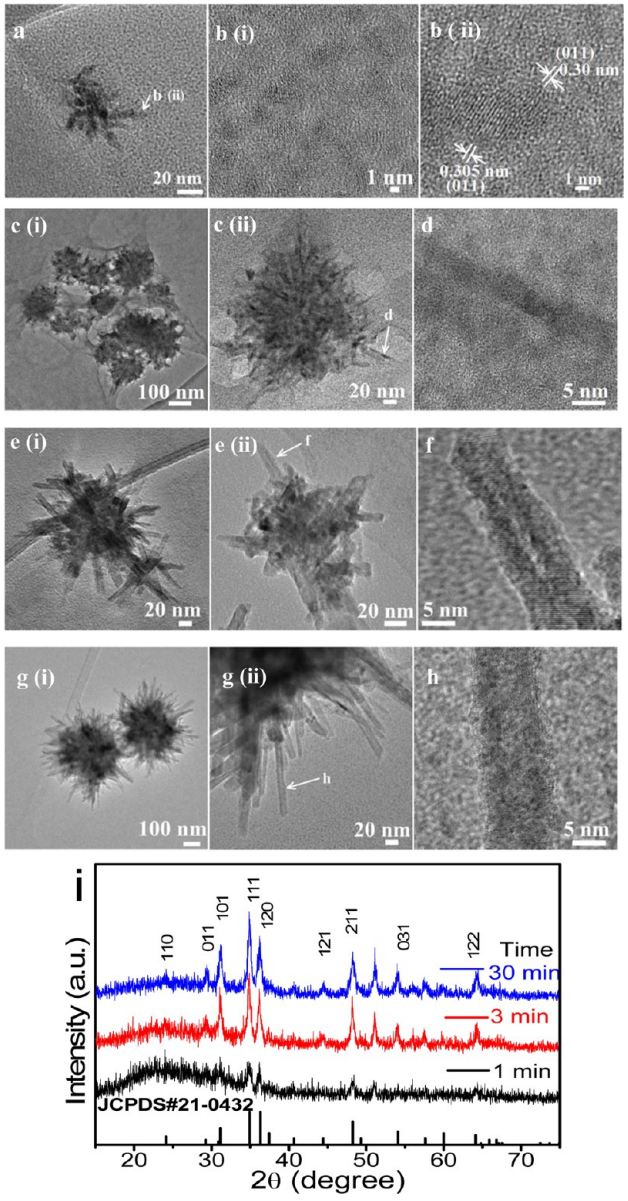


**Figure 8.** (a,c,e,g) TEM and (b,d,f,h) HR-TEM images of reaction aliquots of the intermediates in hedgehog particle synthesis carried out at 175 °C: (a,b) 40 s, (c,d) 1 min, (e,f) 3 min, and (g,h) 5 min. (i) XRD patterns of the hedgehog intermediates for different reaction times.

hypothesized to be the key factor for this multistage self-assembly process for $FeSe_2$ and potentially other types of NPs.[93] The study indicates that the combination of nanoscale anisometry (puck-like shape) and anisotropy (chemical asymmetry of the two basal planes) for the basic building block of the nanoscale assemblies leads to dramatic increase of complexity for the superstructures that can compete in sophistication with biological systems. $FeSe_2$ hedgehog particles can be compared, for instance, to mimivirus that have a diameter of ca 400 nm and star-like shape.[118] Interestingly, the polydispersity of the primary building blocks does not impede the complexity of the self-assembled superstructures.

## METHODS

**Chemicals.** Anhydrous $FeCl_3$ (≥98%, Aldrich), Se powder (100 mesh, 99.5%, Alfa Aesar), 1-dodecanethiol (DT, ≥97%, Fluka),

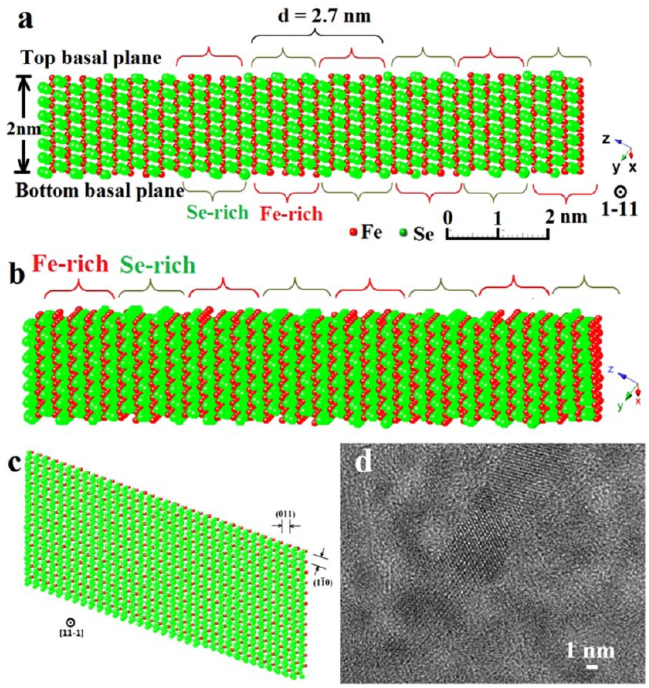


**Figure 9.** (a) Schematic illustration of the periodic Se-rich and Fe-rich stripes on both basal planes of a nanoribbon representing the flattened nanoscroll, viewed from the axis that is perpendicular to [11−1] and parallel to (011). (b) Side view of the nanoribbon from panel (a), showing the periodic Se-rich and Fe-rich stripes on the top basal plane. (c) Top view of the nanoribbon from panel (a). (d) HRTEM image of the nanoribbon formed at the early stage (Figure S23); the atomic structure and dimensions of teh nanoribbon are similar to those in panel (c).

oleylamine (OLA, C18 content 80−90%, Acros), 1-octadecene (ODE, 90%, Aldrich), oleic acid (OA, 99%, Fluka), and chloroform (>99.9%, Aldrich) were all used as received.

**Synthesis of $FeSe_2$ Nanosheets.** For a typical synthetic reaction, anhydrous $FeCl_3$ (0.25 mmol) was first mixed with 3 mL of ODE, 2 mL of OLA, 0.1 mL of DT, and 50 μL of OA in a 50 mL three-neck flask. Under mild stirring, the reaction mixture was slowly heated to 175 °C within 30 min under nitrogen atmosphere until a clear light brown solution was obtained. During this heating process, $Fe^{3+}$ cations were reduced by the mixed system of OLA and DT to form the $Fe^{2+}$ precursor, hereafter named as "solution A". At the same time, the Se precursor solution (i.e., OLA−Se complexes) was prepared by reducing 0.5 mmol of Se powder with the mixture of OLA (0.7 mL) and DT (0.3 mL) at room temperature ($m$OLA + $n$Se + HS−$C_{12}H_{25}$ → $(OLA)_mSe_n$ + $H_{25}C_{12}$−S−S−$C_{12}H_{25}$ ($m \leq n$)),[80,111] hereafter termed "solution B". When the temperature of solution A reached 175 °C, solution B was swiftly injected (~1 s) with a syringe. The solution immediately turned dark, indicating the formation of $FeSe_2$ NPs. Subsequently, the reaction temperature was kept at 175 °C for 30 min to allow the growth of $FeSe_2$ nanosheets. After that, the flask was rapidly cooled to room temperature to harvest the nanosheets products (black precipitate) via centrifugation and then washing three times with chloroform.

**Synthesis of $FeSe_2$ Mesoscale Hedgehog Particles.** In general, the synthetic procedure of $FeSe_2$ mesoscale hedgehog particles is similar to that for nanosheets, except that the volume of DT used was increased to 1 mL from 0.1 mL. In this study, we explored the influence of different parameters on the growth of $FeSe_2$ nanostructures.

**Characterization.** Scanning electron microscopy (SEM) images and energy-dispersive X-ray (EDX) spectroscopy data were acquired by a FEI Nova 200 Nanolab Dualbeam FIB system. Transmission electron microscopy (TEM) and high-resolution transmission electron


DOI: 10.1021/jacs.7b07838
J. Am. Chem. Soc. 2017, 139, 16630−16639

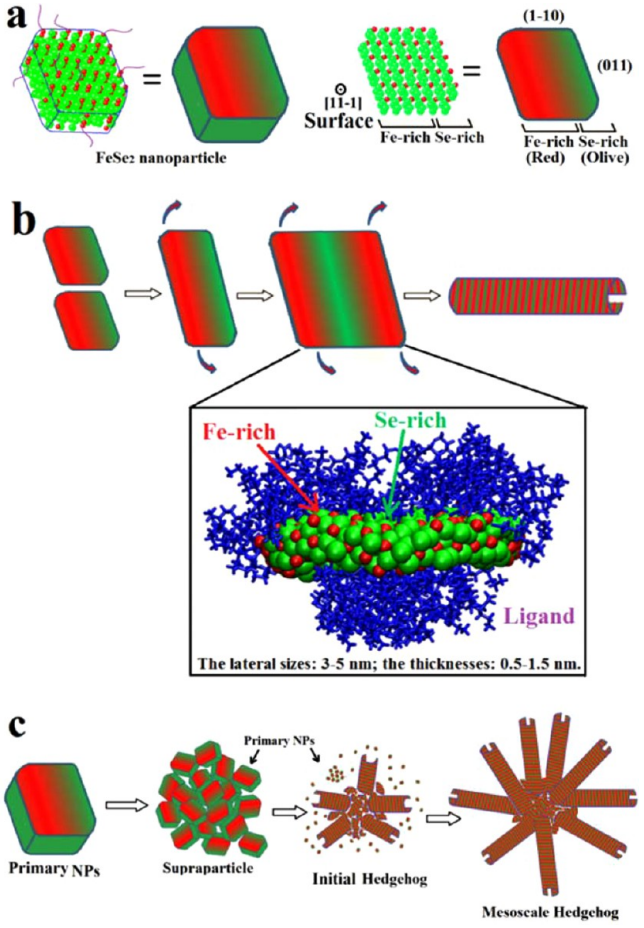


**Figure 10.** (a) Schematics of the primary $FeSe_2$ NPs viewed from the [11−1] axis. (b) Self-assembly of primary NPs and concomitant scrolling; in the inset the image presents the MD simulation snapshot after 20 ns of MD simulation time demonstrating asymmetric distribution of organic ligands on the basal planes for initial aggregates of primary NPs. (c) Schematic illustration of the hypothetical multistage assembly of primary NPs into a mesoscale hedgehog.

microscopy (HR-TEM) images were obtained using a JEOL JEM-3011 microscope operating at 300 kV to further elucidate the size, shape, and crystal structure of the $FeSe_2$ nanocrystals. The 3D reconstruction of electron tomography of the mesoscale hedgehog particles was carried out using a FEI 200 kV Titan Krios cryo-electron microscope, which was equipped with a Gatan Ultrascan 4000 16-megapixel CCD. Atomic force microscopy (AFM) images were obtained using a Veeco Dimension Icon AFM (Bruker), operating in the ScanAsyst air mode. Powder X-ray diffraction (XRD) experiments were performed on a Rigaku rotating anode X-ray diffractometer using Cu K$\alpha$ radiation (1.54 Å) to determine the crystal structure of the nanocrystals. In addition, absorption and photoluminescence (PL) emission spectra were measured at room temperature using an Agilent 8453 UV−vis spectrophotometer and a Jobin Yvon Fluoro Max-3 spectrofluorometer, respectively.

The polydispersity of the hedgehogs was evaluated on the basis of the sizes of TEM images. The outer diameters of the particles were measured and analyzed by Nano Measurer 1.2 software package. The result of the statistical analysis indicates that the size of hedgehogs is 548 ± 21 nm. According to the IUPAC recommendations and accepted conventions in the field,[112] the dispersity index in % is calculated as dispersity index = (standard deviation/mean size).

**Molecular Dynamics Simulations.** An atomistic model of $FeSe_2$ nanosheets with a thickness of 0.6 nm was constructed to represent the primary NPs and to early agglomerates in Figure 4. The ligands were distributed on two surfaces of the nanosheets according to the surface density of the iron atoms. The resulting $FeSe_2$ models were placed in a solvent box containing ODE. We used CHARMM general force-field[113,114] to model the solvent molecules and the ligands. The parameters (bond, angle) for the nanosheet were tuned by using its tensile modulus of elasticity. The charges of iron and selenium of the nanosheet were taken from the calculations of Ataca et al.[115] We performed atomistic MD simulations using Nanoscale Molecular Dynamics (NAMD) software[116] in an isothermal−isobaric ensemble (NPT). Nonbonding interactions were calculated using a cutoff distance of $d$ = 10 Å and long-range electrostatic interactions were calculated by the Particle Mesh Ewald method (PME)[117] with periodic boundary conditions. In the simulations, we used Langevin dynamics with a damping constant of $\gamma_{Lang}$ = 0.1 $ps^{-1}$ and a time step of 2 fs.

**Determination of the Force Field of the Nanosheet.** We built a computational model of a $FeSe_2$ nanosheet with 4 nm length, 4 nm width, and 1.2 nm thickness to calibrate the bond and angle force constants using the tensile and flexural moduli of elasticity. As a part of force filed calibration, we tested the flexural deformation of the nanosheet when two edges of the nanosheet were fixed while a constant downward force was applied at the center of the nanosheet (see Supporting Information, Comment 1). The force is calculated using the equation

$$E_{bend} = \frac{L^3 F}{4wh^3 d}$$

where $L$ is the length, $F$ is applied force, $w$ is width, $h$ is thickness, and $d$ is deflection. The force constants of bonds and angles were adjusted to obtain 1 Å deflection of the nanosheet applying 13.17 nN of force, which correspond to the bending and tensile moduli equal to 305 GPa.

## ■ ASSOCIATED CONTENT

### Supporting Information

The Supporting Information is available free of charge on the ACS Publications website at DOI: 10.1021/jacs.7b07838.

Additional characterizations on the size, shape, crystal structure, and optical properties of the products and the samples obtained by optimizing synthetic conditions or during the assembly process of NPs, including Figures S1−S24 (PDF)

Video File S1, TEM tomography of single $FeSe_2$ hedgehog particle (PPT)

Video File S2, MD simulations of an early $FeSe_2$ NP, view from the (110) edge (PPT)

Video File S3, MD simulations of an early $FeSe_2$ NP, inclined view from the (011) edge (PPT)

Video File S4, atomistic MD simulations of the two primary NPs in close vicinity of each other (AVI)

## ■ AUTHOR INFORMATION


### Corresponding Author

*kotov@umich.edu

### ORCID

Chuanlai Xu: 0000-0002-5639-7102

Petr Král: 0000-0003-2992-9027

Nicholas A. Kotov: 0000-0002-6864-5804


### Notes

The authors declare the following competing financial interest(s): A start-up company is being developed based on this technology with N.A.K. as one of the founders.

## ■ ACKNOWLEDGMENTS

We greatly acknowledge financial assistance by China Scholarship Council to D.D. N.A.K. is thankful to NSF for grants CBET 0932823; CBET 1036672; DMR 1120923; DMR



DOI: 10.1021/jacs.7b07838
J. Am. Chem. Soc. 2017, 139, 16630−16639

1403777; DMR 1411014; CBET 1538180; and CHE 1566460. The work is also partially supported by the U.S. Department of Defense under Grant Awards No. MURI W911NF-12-1-0407. We thank the University of Michigan's Electron Microscopy and Analysis Laboratory (EMAL) for its assistance with electron microscopy. P.K. thanks NSF for the grant DMR-1506886.

## REFERENCES

(1) Archibald, D. D.; Mann, S. *Nature* **1993**, *364*, 430−433.
(2) Mann, S.; Ozin, G. A. *Nature* **1996**, *382*, 313−318.
(3) Yang, H.; Coombs, N.; Ozin, G. A. *Nature* **1997**, *386*, 692−695.
(4) Kotov, N. A.; Meldrum, F. C.; Wu, C.; Fendler, J. H. *J. Phys. Chem.* **1994**, *98*, 2735−2738.
(5) Meldrum, F. C.; Kotov, N. A.; Fendler, J. H. *Langmuir* **1994**, *10*, 2035−2040.
(6) Tang, Z.; Kotov, N. A.; Giersig, M. *Science* **2002**, *297*, 237−240.
(7) Tang, Z.; Zhang, Z.; Wang, Y.; Glotzer, S. C.; Kotov, N. A. *Science (Washington, DC, U. S.)* **2006**, *314*, 274−278.
(8) Srivastava, S.; Santos, A.; Critchley, K.; Kim, K.-S.; Podsiadlo, P.; Sun, K.; Lee, J.; Xu, C.; Lilly, G. D.; Glotzer, S. C.; et al. *Science* **2010**, *327*, 1355−1359.
(9) Mohanan, J. L.; Arachchige, I. U.; Brock, S. L. *Science* **2005**, *307*, 397−400.
(10) Gaponik, N.; Herrmann, A.-K.; Eychmüller, A. *J. Phys. Chem. Lett.* **2012**, *3*, 8−17.
(11) Xia, Y.; Nguyen, T. D.; Yang, M.; Lee, B.; Santos, A.; Podsiadlo, P.; Tang, Z.; Glotzer, S. C.; Kotov, N. A. *Nat. Nanotechnol.* **2011**, *6*, 580−587.
(12) Piccinini, E.; Pallarola, D.; Battaglini, F.; Azzaroni, O. *Mol. Syst. Des. Eng.* **2016**, *1*, 155−162.
(13) Ge, J.; Hu, Y.; Yin, Y. *Angew. Chem., Int. Ed.* **2007**, *46*, 7428−7431.
(14) Ramsden, J. J. *Proc. R. Soc. London, Ser. A* **1987**, *413*, 407−414.
(15) Murray, C. B.; Kagan, C. R.; Bawendi, M. G. *Science (Washington, DC, U. S.)* **1995**, *270*, 1335−1338.
(16) Shenton, W.; Pum, D.; Sleytr, U. B.; Mann, S. *Nature* **1997**, *389*, 585−587.
(17) Pileni, M. P. *Phys. Chem. Chem. Phys.* **2010**, *12*, 11821.
(18) Macfarlane, R. J.; Lee, B.; Jones, M. R.; Harris, N.; Schatz, G. C.; Mirkin, C. A. *Science* **2011**, *334*, 204−208.
(19) Tan, R.; Zhu, H.; Cao, C.; Chen, O. *Nanoscale* **2016**, *8*, 9944−9961.
(20) Shanbhag, S.; Kotov, N. A. *J. Phys. Chem. B* **2006**, *110*, 12211−12217.
(21) Sinyagin, A.; Belov, A.; Kotov, N. A. *Modell. Simul. Mater. Sci. Eng.* **2005**, *13*, 389−399.
(22) Bishop, K. J. M.; Wilmer, C. E.; Soh, S.; Grzybowski, B. A. *Small* **2009**, *5*, 1600−1630.
(23) Min, Y.; Akbulut, M.; Kristiansen, K.; Golan, Y.; Israelachvili, J. *Nat. Mater.* **2008**, *7*, 527−538.
(24) Silvera Batista, C. A.; Larson, R. G.; Kotov, N. A. *Science (Washington, DC, U. S.)* **2015**, *350*, 1242477.
(25) Jun, Y.; Choi, J.; Cheon, J. *Angew. Chem., Int. Ed.* **2006**, *45*, 3414−3439.
(26) Dykman, L.; Khlebtsov, N. *Chem. Soc. Rev.* **2012**, *41*, 2256−2282.
(27) Rodríguez-Lorenzo, L.; de la Rica, R.; Álvarez-Puebla, R. A.; Liz-Marzán, L. M.; Stevens, M. M. *Nat. Mater.* **2012**, *11*, 604−607.
(28) Xia, Y.; Xiong, Y.; Lim, B.; Skrabalak, S. E. *Angew. Chem., Int. Ed.* **2009**, *48*, 60−103.
(29) Jiang, L.; Feng, L. *Bioinspired Intelligent Nanostructured Interfacial Materials*; Chemical Industry Press, 2010; Vol. *38*.
(30) Dorrer, C.; Rühe, J. *Adv. Mater.* **2008**, *20*, 159−163.
(31) Zhang, H.; Lamb, R.; Lewis, J. *Sci. Technol. Adv. Mater.* **2005**, *6*, 236−239.
(32) Bahng, J. H.; Yeom, B.; Wang, Y.; Tung, S. O.; Hoff, J. D.; Kotov, N. *Nature* **2015**, *517*, 596−599.
(33) Ballister, E. R.; Lai, A. H.; Zuckermann, R. N.; Cheng, Y.; Mougous, J. D. *Proc. Natl. Acad. Sci. U. S. A.* **2008**, *105*, 3733−3738.
(34) Klug, A. *Philos. Trans. R. Soc., B* **1999**, *354*, 531−535.
(35) Kotov, N. A. *Science (Washington, DC, U. S.)* **2010**, *330*, 188−189.
(36) Sleytr, U. B.; Huber, C.; Ilk, N.; Pum, D.; Schuster, B.; Egelseer, E. M. *FEMS Microbiol. Lett.* **2007**, *267*, 131−144.
(37) Duda, R. L. *Cell* **1998**, *94*, 55−60.
(38) Serpell, L. C. *Biochim. Biophys. Acta, Mol. Basis Dis.* **2000**, *1502*, 16−30.
(39) Van Gerven, N.; Klein, R. D.; Hultgren, S. J.; Remaut, H. *Trends Microbiol.* **2015**, *23*, 693−706.
(40) Zhao, G.; Perilla, J. R.; Yufenyuy, E. L.; Meng, X.; Chen, B.; Ning, J.; Ahn, J.; Gronenborn, A. M.; Schulten, K.; Aiken, C.; et al. *Nature* **2013**, *497*, 643−646.
(41) Xia, Y.; Xiong, Y.; Lim, B.; Skrabalak, S. E. *Angew. Chem., Int. Ed.* **2009**, *48*, 60−103.
(42) Peng, X.; Manna, L.; Yang, W.; Wickham, J.; Scher, E.; Kadavanich, A.; Alivisatos, A. P. *Nature* **2000**, *404*, 59−61.
(43) Lohse, S. E.; Murphy, C. J. *J. Am. Chem. Soc.* **2012**, *134*, 15607−15620.
(44) Koh, W.; Bartnik, A. C.; Wise, F. W.; Murray, C. B. *J. Am. Chem. Soc.* **2010**, *132*, 3909−3913.
(45) Schliehe, C.; Juarez, B. H.; Pelletier, M.; Jander, S.; Greshnykh, D.; Nagel, M.; Meyer, A.; Foerster, S.; Kornowski, A.; Klinke, C.; Weller, H. *Science* **2010**, *329*, 550−553.
(46) Srivastava, S.; Santos, A.; Critchley, K.; Kim, K.-S.; Podsiadlo, P.; Sun, K.; Lee, J.; Xu, C.; Lilly, G. D.; Glotzer, S. C.; et al. *Science* **2010**, *327*, 1355−1359.
(47) Cho, K.-S.; Talapin, D. V.; Gaschler, W.; Murray, C. B. *J. Am. Chem. Soc.* **2005**, *127*, 7140−7147.
(48) Jia, G.; Sitt, A.; Hitin, G. B.; Hadar, I.; Bekenstein, Y.; Amit, Y.; Popov, I.; Banin, U. *Nat. Mater.* **2014**, *13*, 301−307.
(49) Breen, T. L. *Science (Washington, DC, U. S.)* **1999**, *284*, 948−951.
(50) Grzelczak, M.; Vermant, J.; Furst, E. M.; Liz-Marzán, L. M. *ACS Nano* **2010**, *4*, 3591−3605.
(51) Kim, Y.; Zhu, J.; Yeom, B.; Di Prima, M.; Su, X.; Kim, J.-G.; Yoo, S. J.; Uher, C.; Kotov, N. A. *Nature* **2013**, *500*, 59−63.
(52) Xu, L.; Ma, W.; Wang, L.; Xu, C.; Kuang, H.; Kotov, N. A. *Chem. Soc. Rev.* **2013**, *42*, 3114−3126.
(53) Penn, R. L.; Banfield, J. F. *Science* **1998**, *281*, 969−971.
(54) Gong, M.; Kirkeminde, A.; Ren, S.; et al. *Sci. Rep.* **2013**, *3*, 1174−1177.
(55) Polleux, J.; Pinna, N.; Antonietti, M.; Niederberger, M. *J. Am. Chem. Soc.* **2005**, *127*, 15595−15601.
(56) Xu, J.; Jang, K.; Lee, J.; Kim, H. J.; Jeong, J.; Park, J.-G.; Son, S. U. *Cryst. Growth Des.* **2011**, *11*, 2707−2710.
(57) Yuan, B.; Hou, X.; Han, Y.; Luan, W.; Tu, S. *New J. Chem.* **2012**, *36*, 2101.
(58) Shi, W.; Zhang, X.; Che, G.; Fan, W.; Liu, C. *Chem. Eng. J.* **2013**, *215−216*, 508−516.
(59) Huang, S.; He, Q.; Chen, W.; Zai, J.; Qiao, Q.; Qian, X. *Nano Energy* **2015**, *15*, 205−215.
(60) Wang, W.; Pan, X.; Liu, W.; Zhang, B.; Chen, H.; Fang, X.; Yao, J.; Dai, S. *Chem. Commun.* **2014**, *50*, 2618−2620.
(61) Zhang, K.; Hu, Z.; Liu, X.; Tao, Z.; Chen, J. *Adv. Mater.* **2015**, *27*, 3305−3309.
(62) Mao, X.; Kim, J. G.; Han, J.; Jung, H. S.; Lee, S. G.; Kotov, N. A.; Lee, J. *J. Am. Chem. Soc.* **2014**, *136*, 7189−7192.
(63) Wei, C.; Bai, Y.; Deng, A.; Bao, Y. *Nanotechnology* **2016**, *27*, 165702.
(64) Xu, X.; Ge, Y.; Wang, M.; Zhang, Z.; Dong, P.; Baines, R.; Ye, M.; Shen, J. *ACS Appl. Mater. Interfaces* **2016**, *8*, 18036−18042.
(65) Di Giovanni, C.; Wang, W.-A.; Nowak, S.; Grenèche, J.-M.; Lecoq, H.; Mouton, L.; Giraud, M.; Tard, C. *ACS Catal.* **2014**, *4*, 681−687.


DOI: 10.1021/jacs.7b07838
J. Am. Chem. Soc. 2017, 139, 16630−16639

(66) Takeuchi, T.; Kageyama, H.; Nakanishi, K.; Inada, Y.; Katayama, M.; Ohta, T.; Senoh, H.; Sakaebe, H.; Sakai, T.; Tatsumi, K.; et al. *J. Electrochem. Soc.* **2012**, *159*, A75.
(67) Yuan, B.; Luan, W.; Tu, S.; Wu, J. *New J. Chem.* **2015**, *39*, 3571−3577.
(68) Han, W.; Gao, M. *Cryst. Growth Des.* **2008**, *8*, 1023−1030.
(69) Bai, Y.; Yeom, J.; Yang, M.; Cha, S. H.; Sun, K.; Kotov, N. A. *J. Phys. Chem. C* **2013**, *117*, 2567−2573.
(70) Wadia, C.; Alivisatos, A. P.; Kammen, D. M. *Environ. Sci. Technol.* **2009**, *43*, 2072−2077.
(71) Cummins, D. R.; Russell, H. B.; Jasinski, J. B.; Menon, M.; Sunkara, M. K. *Nano Lett.* **2013**, *13*, 2423−2430.
(72) Liu, H.; Chi, D. *Procedia Eng.* **2016**, *141*, 32−37.
(73) Shi, X.; Sun, K.; Balogh, L. P.; Baker, J. R. *Nanotechnology* **2006**, *17*, 4554−4560.
(74) Wang, Y.-X.; Yang, J.; Chou, S.-L.; Liu, H. K.; Zhang, W.; Zhao, D.; Dou, S. X. *Nat. Commun.* **2015**, *6*, 8689.
(75) Chin, P. P.; Ding, J.; Yi, J. B.; Liu, B. H. *J. Alloys Compd.* **2005**, *390*, 255−260.
(76) Xu, C.; Zeng, Y.; Rui, X.; Xiao, N.; Zhu, J.; Zhang, W.; Chen, J.; Liu, W.; Tan, H.; Hng, H. H.; et al. *ACS Nano* **2012**, *6*, 4713−4721.
(77) Querejeta-Fernàndez, A.; Hernàndez-Garrido, J. C.; Yang, H.; Zhou, Y.; Varela, A.; Parras, M.; Calvino-Gàmez, J. J.; Gonzàlez-Calbet, J. M.; Green, P. F.; Kotov, N. A. *ACS Nano* **2012**, *6*, 3800−3812.
(78) Zhou, H.; Kim, J.-P.; Bahng, J. H.; Kotov, N. A.; Lee, J. *Adv. Funct. Mater.* **2014**, *24*, 1439−1448.
(79) Lucas, J. M.; Tuan, C. C.; Lounis, S. D.; Britt, D. K.; Qiao, R.; Yang, W.; Lanzara, A.; Alivisatos, A. P. *Chem. Mater.* **2013**, *25*, 1615−1620.
(80) Liu, Y.; Yao, D.; Shen, L.; Zhang, H.; Zhang, X.; Yang, B. *J. Am. Chem. Soc.* **2012**, *134*, 7207−7210.
(81) Boles, M. A.; Engel, M.; Talapin, D. V. *Chem. Rev.* **2016**, *116*, 11220−11289.
(82) Liz-Marzán, L. M. *Langmuir* **2006**, *22*, 32−41.
(83) Park, J. I.; Nguyen, T. D.; de Queirós Silveira, G.; Bahng, J. H.; Srivastava, S.; Zhao, G.; Sun, K.; Zhang, P.; Glotzer, S. C.; Kotov, N. A. *Nat. Commun.* **2014**, *5*, 3593.
(84) Hirai, K.; Yeom, B.; Chang, S.; Chi, H.; Mansfield, J. F.; Lee, B.; Lee, S.; Uher, C.; Kotov, N. A. *Angew. Chem., Int. Ed.* **2015**, *54*, 8966.
(85) Bouet, C.; Mahler, B.; Nadal, B.; Abecassis, B.; Tessier, M. D.; Ithurria, S.; Xu, X.; Dubertret, B. *Chem. Mater.* **2013**, *25*, 639−645.
(86) Zhang, X.; Liu, Q.; Meng, L.; Wang, H.; Bi, W.; Peng, Y.; Yao, T.; Wei, S.; Xie, Y. *ACS Nano* **2013**, *7*, 1682−1688.
(87) Du, Y.; Yin, Z.; Zhu, J.; Huang, X.; Wu, X.-J.; Zeng, Z.; Yan, Q.; Zhang, H. *Nat. Commun.* **2012**, *3*, 1177.
(88) Zhou, Y.; Marson, R. L.; Van Anders, G.; Zhu, J.; Ma, G.; Ercius, P.; Sun, K.; Yeom, B.; Glotzer, S. C.; Kotov, N. A. *ACS Nano* **2016**, *10*, 3248−3256.
(89) Yang, M.; Chan, H.; Zhao, G.; Bahng, J. H.; Zhang, P.; Král, P.; Kotov, N. A. *Nat. Chem.* **2017**, *9*, 287−294.
(90) Nor, Y. A.; Zhou, L.; Meka, A. K.; Xu, C.; Niu, Y.; Zhang, H.; Mitter, N.; Mahony, D.; Yu, C. *Adv. Funct. Mater.* **2016**, *26*, 5408−5418.
(91) Keten, S.; Xu, Z.; Ihle, B.; Buehler, M. J. *Nat. Mater.* **2010**, *9*, 359−367.
(92) Xia, Y.; Tang, Z. *Chem. Commun. (Cambridge, U. K.)* **2012**, *48*, 6320−6336.
(93) Fu, Q.; Sheng, Y.; Tang, H.; Zhu, Z.; Ruan, M.; Xu, W.; Zhu, Y.; Tang, Z. *ACS Nano* **2015**, *9*, 172−179.
(94) Ye, X.; Chen, J.; Engel, M.; Millan, J. A.; Li, W.; Qi, L.; Xing, G.; Collins, J. E.; Kagan, C. R.; Li, J.; et al. *Nat. Chem.* **2013**, *5*, 466−473.
(95) Viculis, L. M.; Mack, J. J.; Kaner, R. B. *Science* **2003**, *299*, 1361.
(96) Ye, C.; Bando, Y.; Shen, G.; Golberg, D. *Angew. Chem., Int. Ed.* **2006**, *45*, 4922−4926.
(97) Kuroda, Y.; Ito, K.; Itabashi, K.; Kuroda, K. *Langmuir* **2011**, *27*, 2028−2035.
(98) Ma, G.; Zhou, Y.; Li, X.; Sun, K.; Liu, S.; Hu, J.; Kotov, N. A. *ACS Nano* **2013**, *7*, 9010−9018.
(99) Zhang, G.; Sun, S.; Li, R.; Zhang, Y.; Cai, M.; Sun, X. *Chem. Mater.* **2010**, *22*, 4721−4727.
(100) Cendula, P.; Kiravittaya, S.; Mönch, I.; Schumann, J.; Schmidt, O. G. *Nano Lett.* **2011**, *11*, 236−240.
(101) Hoshyargar, F.; Yella, A.; Panthöfer, M.; Tremel, W. *Chem. Mater.* **2011**, *23*, 4716−4720.
(102) Patra, N.; Wang, B.; Král, P. *Nano Lett.* **2009**, *9*, 3766−3771.
(103) Li, J.; Zhang, J.; Gao, W.; Huang, G.; Di, Z.; Liu, R.; Wang, J.; Mei, Y. *Adv. Mater.* **2013**, *25*, 3715−3721.
(104) Wang, Y.; Wise, A. K.; Tan, J.; Maina, J. W.; Shepherd, R. K.; Caruso, F. *Small* **2014**, *10*, 4243.
(105) Zhou, Y.; Marson, R. L.; Van Anders, G.; Zhu, J.; Ma, G.; Ercius, P.; Sun, K.; Yeom, B.; Glotzer, S. C.; Kotov, N. A. *ACS Nano* **2016**, *10*, 3248−3256.
(106) Biggs, S.; Chow, M. K.; Zukoski, C. F.; Grieser, F. *J. Colloid Interface Sci.* **1993**, *160*, 511−513.
(107) Fojtik, A.; Weller, H.; Koch, U.; Henglein, A. *Berichte der Bunsengesellschaft für Phys. Chemie* **1984**, *88*, 969−977.
(108) Luo, W.; Zhu, C.; Su, S.; Li, D.; He, Y.; Huang, Q.; Fan, C. *ACS Nano* **2010**, *4*, 7451−7458.
(109) Zhang, Z.; Glotzer, S. C. *Nano Lett.* **2004**, *4*, 1407−1413.
(110) Zhang, Q.; Wang, W.; Kong, X.; Mendes, R. G.; Fang, L.; Xue, Y.; Xiao, Y.; Rümmeli, M. H.; Chen, S.; Fu, L. *J. Am. Chem. Soc.* **2016**, *138*, 11101−11104.
(111) Deng, D.; Qu, L.; Achilefu, S.; Gu, Y.; et al. *Chem. Commun.* **2013**, *49*, 9494.
(112) Daniel, M. C.; Astruc, D. *Chem. Rev.* **2004**, *104*, 293−346.
(113) Vanommeslaeghe, K.; Hatcher, E.; Acharya, C.; Kundu, S.; Zhong, S.; Shim, J.; Darian, E.; Guvench, O.; Lopes, P.; Vorobyov, I.; Mackerell, A. D.; et al. *J. Comput. Chem.* **2010**, *31*, 671−690.
(114) Yu, W.; He, X.; Vanommeslaeghe, K.; MacKerell, A. D. *J. Comput. Chem.* **2012**, *33*, 2451−2468.
(115) Ataca, C.; Şahin, H.; Ciraci, S. *J. Phys. Chem. C* **2012**, *116*, 8983−8999.
(116) Phillips, J. C.; Braun, R.; Wang, W.; Gumbart, J.; Tajkhorshid, E.; Villa, E.; Chipot, C.; Skeel, R. D.; Kalé, L.; Schulten, K. *J. Comput. Chem.* **2005**, *26*, 1781−1802.
(117) Darden, T.; York, D.; Pedersen, L. *J. Chem. Phys.* **1993**, *98*, 10089.
(118) Zauberman, N.; Mutsafi, Y.; Halevy, D. B.; Shimoni, E.; Klein, E.; Xiao, C.; Sun, S.; Minsky, A. *PLoS Biol.* **2008**, *6*, e114.


DOI: 10.1021/jacs.7b07838
*J. Am. Chem. Soc.* 2017, 139, 16630−16639